University of Groningen

Bachelor Thesis

The effect of hydrodynamical shielding and magnetic draping on the survival of High-Velocity Clouds.

Author:
Florian Bennebroek Evertsz'

Supervisors:
Dr. Asger Grønnow
Prof. Dr. Filippo Fraternali

July 3, 2020

1 ABSTRACT

In this report the survival times of high-velocity clouds in the galactic halo are estimated for clouds subject to different protective mechanisms. Using the PLUTO code, 4 different simulations are run of clouds travelling through the halo. The first simulation consists of a single cold cloud travelling through a hot medium (representing the galactic halo). The second simulation shows three clouds of the same size travelling through the halo, in this situation the lifetime of the second and third cloud improves due to the shielding effect of the first cloud. The third simulation displays a single cloud moving through the halo similarly to the first simulation but in this case a magnetic field component is added perpendicular to the motion of the cloud. This increases the survival time of the cloud greatly. The final simulation combines the shielding effect of multiple clouds and the magnetic field. The destruction of the clouds is quantified and compared by determining the fraction of the cloud material that mixes with the hot gas at different times. I find the magnetic field to have the biggest influence on the clouds survival while the addition of other clouds provided less protection.

2   ACKNOWLEDGEMENTS

I would like to thank my supervisor, Dr. Asger Grønnow, for everything he has helped me with while writing this bachelor thesis. I also thank my other supervisor, Prof. Dr. Filippo Fraternali, for the opportunity and for guiding me through the project.

Contents

3 INTRODUCTION

3.1 GALAXY HALO COMPOSITION

During the lifetime of a star forming galaxy, gas continuously flows in and out of its disk. The galactic halo forms the region of space between the intergalactic medium (IGM) and the star-forming disk of the galaxy and is a collection of these in- and out flowing gasses as well as a large amount of stable hot gas. This causes the galactic halo to contain gas in several different states: neutral hydrogen gas, warm gas and hot gas. The gas flows creating these different states are caused by different physical processes in- and outside the galaxy: accretion from the IGM, satellite accretion and feedback from the star forming regions and the active galactic nucleus (AGN) [Putman et al., 2012].

3.1.1 High-velocity clouds

The neutral hydrogen gas has a temperature of 10^4 K or lower and can be observed through the 21-cm line in emission. This yields a measurement of the hydrogen spin temperature from which the kinetic gas temperature can be inferred [Wakker and van Woerden, 1997]. It mostly consists of high velocity clouds (HVC), although a considerable amount of HVCs are also made up of cold ionized gas. Even fully ionized HVCs have been found [Lehner et al., 2012]. The gas in these HVCs is photoionized by light from stars and so this gas has the same temperature as neutral gas. HVCs are the coldest and more dense parts of the halo. Their sizes range from 1000 degree^2 on the sky down to smaller than the resolution of the observations [Putman et al., 2012]. Their velocity ranges from -400 to 400 km s^{-1} [Olano, 2008]. Larger clouds are often found to be consisting of multiple smaller clouds when observed with increased resolution. The clouds are grouped together according to their expected origin. The largest groups are the Magellanic stream (MS), Complex C, Complex A and the Leading arm (LA) all visible in figure 1. To determine physical properties of HVCs their distance needs to be known. The best way to measure the distance to a HVC is by searching for absorption lines in the spectrum of a star at known distance in the direction of the cloud. When absorption lines are detected, the cloud must be in front of the star giving an upper limit to the distance. In the same way, a lower limit can be found by studying stars in the same direction as the cloud which do not show any absorption lines [Thom et al., 2008]. Using this method most HVCs have been found to be at a distance of 2 - 15 kpc with the exception of the MS and LA. which are found to be at 55 kpc and can extend to 100-150 kpc in case of the MS [Putman et al., 2012].
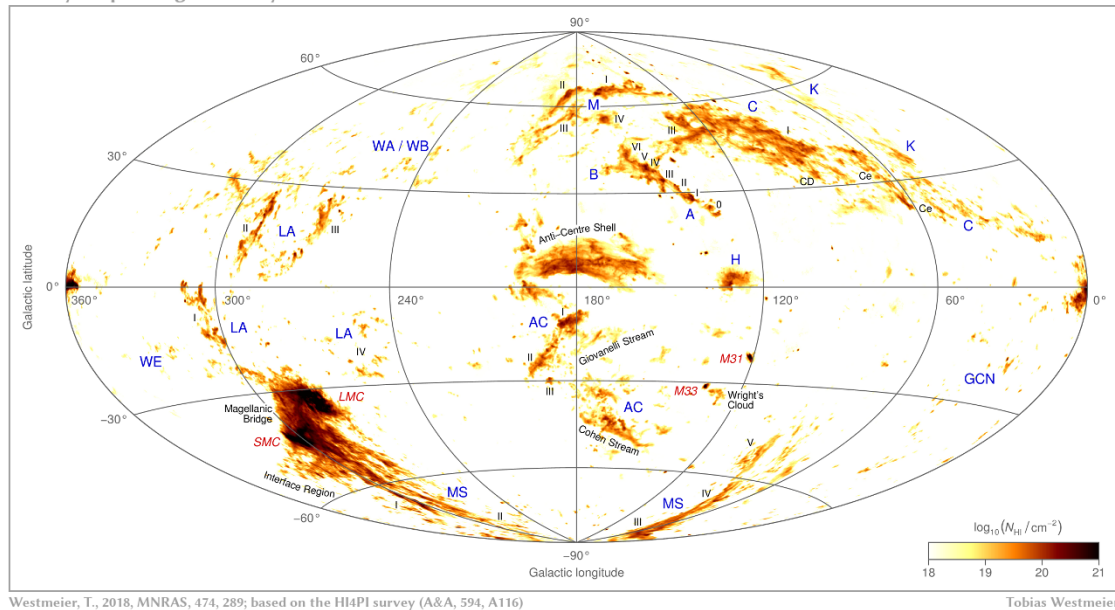
Figure 1: The high velocity cloud distribution in the Milky Way halo [Westmeier, 2018]

Knowing the distances and column densities of HVCs allows us to estimate their mass. The total mass of all HVCs in the Milky Way combined is thought to be of the order of 10^7 Solar masses while the Magellanic system will contribute another 3×10^8 solar masses [Putman et al., 2012]. Single cloud masses are estimated at $10^5 - 10^6$ solar masses with a volume density of $0.05 - 0.15$ cm^3 [Putman et al., 2012]. The pressure of HVCs varies with their position in the halo: since the clouds are in pressure equilibrium with the hot halo, clouds in outer less pressurized parts of the halo are less dense than those closer to the galactic disk. The warm halo gas has temperatures between 10^4 and 10^5 K and can therefore be observed in emission through the Hα line. Most of the warm gas has been detected around the HI gas in all HVCs with the exception of the LA. The ionized warm gas contributes about the same mass to HVC complexes as the HI gas ($3 - 4 \times 10^7$ Solar masses) [Putman et al., 2012]. The detection of halo gas is difficult because of the low column densities [Sancisi et al., 2008]. In the Milky Way it is mostly done by searching for gas that has a velocity that does not match the velocity distribution of the disk by studying absorption lines [Thom et al., 2008]. Depending on the temperature of the gas, different lines in the spectrum can be studied. The advantage of searching for halo gas through absorption lines over other methods is that it is sensitive to a large range of densities. However to measure the absorption lines of a cloud a very bright background source, like a quasar, is needed. These objects are quite rare and so only very specific parts of the Milky Way's halo can be observed this way. External galaxies often have only one line of sight. Therefore most maps of the halo made using this detection technique are a statistical average of gas from many different galaxies combined to form one complete image [Tumlinson et al., 2017].

5

3.1.2 Hot halo gas

The hot halo gas has temperatures of 10^6 K and higher and is detected by observing X-ray emission lines [Tumlinson et al., 2017]. It originates from feedback mechanisms and shock-heated gas from the IGM. Most of the hot gas is located a couple of kpc from the disk although there is evidence for a lower density medium of hot gas stretching up to about 100 kpc. The main evidence for the existence of this medium is that this medium helps to strip satellite galaxies of their cold gas at large radii (100 kpc). As well as that it supports and destroys cold halo clouds at large distances from the disk. Physical properties of the hot halo are very uncertain. However, the mass is exstimated to be $6.5^{+13.2}_{-1.3} \times 10^9$ solar masses within a 160 kpc radius [Miller and Bregman, 2013]. Estimates for the density range from 10^{-2} in the inner halo to 10^{-5} cm^{-3} in the outer halo [Tepper-García et al., 2019].

3.2 GALAXY HALO EVOLUTION

Cosmological simulations have shown that galaxies can reach a stationary state where gas outflows and star formation rates balance out against the accretion of gas [Finlator and Davé, 2008]. Some balance is required for a galaxy to keep forming stars because the time required to form stars from the existing gas (in galaxies) is much shorter than the Hubble time. Without this balance, there would be a lot less star formation present in galaxies and in some galaxies star formation would already have ended. Given that this is not happening implies that a continuous inflow of gas is feeding the galaxy such that it keeps producing stars [Tumlinson et al., 2017]. The same equilibrium is also found in the chemical composition of galaxies. The inflow of intergalactic gas along filaments has relatively low metallicity which is compensated by the enriched gas from star formation [Kacprzak, 2016].
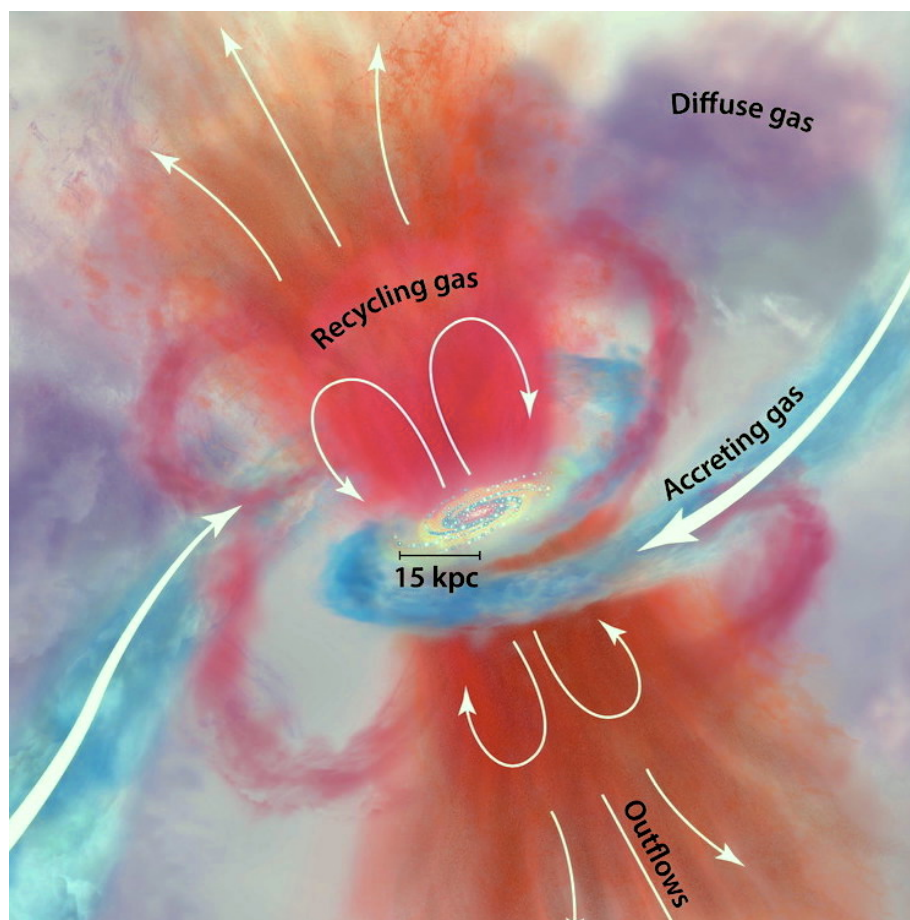

Figure 2: The in- and outflow of gas in a spiral galaxy [Tumlinson et al., 2017]

3.2.1 Satellite accretion

Satellite accretion occurs when a satellite galaxy penetrates the halo of a larger spiral galaxy. The smaller galaxy gets stripped of its gas which is then left behind in the halo of the spiral galaxy. Observations have shown that roughly 40% of galaxies similar in size to the Milky Way contain a large satellite galaxy (0.1 L_{gal}) within their virial radius. Most satellite galaxies are much smaller, but they provide the galaxy with a lot less gas and so their combined effect is smaller than the few larger satellite galaxies. For example, 30-50% of the HI gas in the Milky Way originates from the Magellanic clouds and streams. In comparison, all observed small satellite galaxies in the Milky Way contribute around 1% of the HI mass [Putman et al., 2012]. This accreted gas will at some point supply the disk which loses gas to outflows and star formation. However, since most satellites lose their gas more than 20 kpc from the galactic center, most of the gas is likely to heat up due to the interaction with the hot halo gas and remain in the galactic halo before cooling down and reaching the disk [Putman et al., 2012]. This results in a multi-phase halo consistent with observations throughout the Milky Way and external galaxies [Almeida, 2016]. The satellite gas present in the halo, on average, has a higher radial velocity than the halo itself. This is the main clue for detecting HVCs originating from satellite accretion.

3.2.2 Accretion from the IGM

Most gas in the Universe lies within the intergalactic medium where it largely resides in filaments that form the cosmic web. Galaxies often form around intersections of these filaments and are supplied with gas from the filaments due to their gravitational pull. In case of the Milky Way, About 70% of gas enters the halo in this way [Putman et al., 2012]. Since there is no observational evidence for this process, one has to rely on theoretical models. These indicate that there are two modes of accretion from the IGM: cold and hot mode accretion. During cold mode accretion the gas flows into the galaxy directly from intergalactic filaments, this process dominates in small galaxies (baryonic halo mass $\leq 10^{11.4}$) [Keres et al., 2005] at high redshifts. Hot mode accretion dominates in large galaxies and at low redshifts as can be seen in figure 3. In this case the incoming gas is heated by shocks where the kinetic energy of the gas is converted into thermal energy due to the compression caused by the surrounding halo gas. Gas accreted in
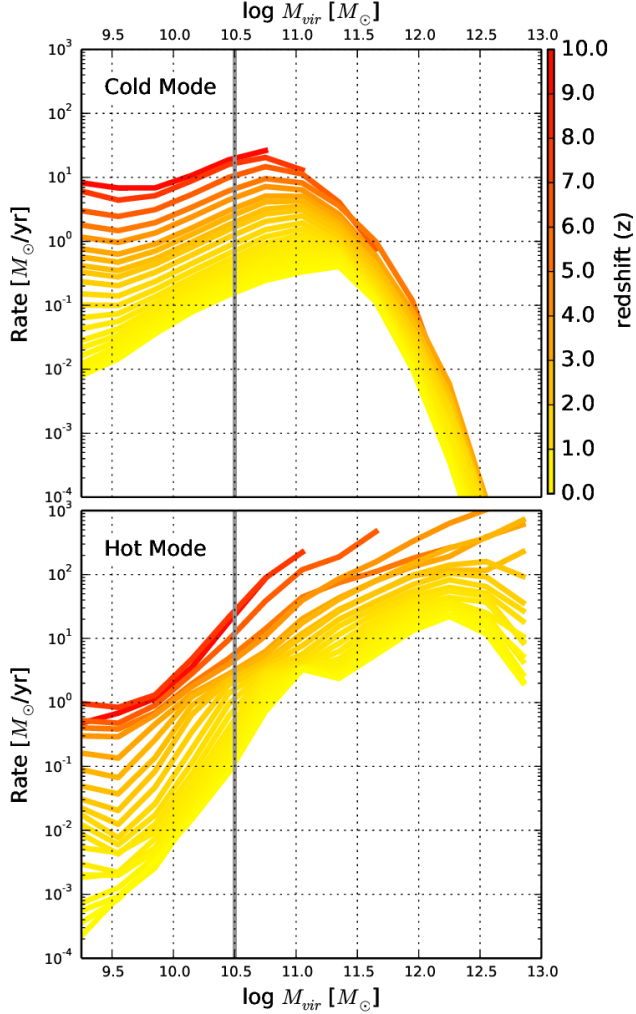

Figure 3: Cold and Hot mode accretion as function of mass, the gray line indicates the mass where cold and hot mode accretion contribute the same amount of gas. [Cousin et al., 2019]

these ways usually become part of the warm and warm-hot medium of the halo when their temperature remains below 10^5K, when the gas is heated to higher temperatures it becomes part of the hot medium.

9

3.2.3 Feedback

Physical processes inside the disk can influence the structure and composition of the halo as well. These processes include radiation of young stars, supernovae and active galactic nuclei. Young stars in the galaxy disk radiate ionizing photons into the galactic halo. Most of these photons are radiated away normal to the disk, causing parts of the halo to heat up and ionize. Gas outflows caused by supernovae and AGNs are the most important feedback processes that alter the halo composition. Somewhere between 10-25% of the HI and warm-ionized gas of the galaxy is carried into the halo by these events [Marasco et al., 2012]. these clouds ejected by feedback are stripped of their gas due to Kelvin-Helmholtz instabilities between the clouds and the surrounding hot halo. In the turbulent wake of the cloud, the high metallicity gas mixes with the halo gas increasing the density and metallicity. This results in the surrounding halo gas condensing into the wake increasing the amount of cold gas [Marasco et al., 2012]. Eventually this cold gas returns to the disk completing the 'fountain'. This process, where gas is ejected and then returned to the star forming disk, is called fountain accretion.

3.3 SURVIVAL OF COLD CLOUDS

HVCs fall apart in the halo in a couple hundred million years, primarily due to Kelvin-Helmholtz instabilities, unless they are supported by some physical mechanism. The exact lifetime of a cloud depends on its velocity, density and mass. This can be seen when estimating the time needed for Kelvin-Helmholtz instabilities to form [Putman et al., 2012]: $t_{KH} \propto \chi^{\frac{1}{2}} R_c / v_{rel}$. Here χ is the density ratio between the halo and cloud gas, R_c is the length (Diameter when assuming a spherical cloud) of the cloud and v_{rel} is the velocity of the cloud relative to the hot gas. The Kelvin-Helmholtz instabilities cause gas to ablate from the edges of the cloud and make a trail of lower density material. HVCs reach their high velocities because they are accelerated by the gravitational force of the galaxy. However, they often reach velocities higher than possible in their expected lifetime. This indicates that the HVCs are partially shielded by some mechanism present in the halo. There are multiple theories which could result in the prolonged lifetime of HVCs: the presence of dark matter, a magnetic field or the shielding effect of other cloud material. Dark matter could increase the lifetime of a HVC by about a gigayear [Putman et al., 2012]. However, evidence suggest that there is no dark matter present in and around HVCs. The halo magnetic field is another option and is studied in this report. Although very weak (¡ 1 μG) [Sun and Reich, 2010], it could play an important role in preventing the destruction of HVCs. The high density cloud acts as a barrier to the magnetic field. This makes the magnetic field drape around the cloud (when perpendicular to the motion of the cloud) which increases the strength of the field surrounding the cloud. This strong magnetic field increases the time needed for Kelvin-Helmholtz instabilities to form. The magnetic field is usually split in a disk and halo field, the halo field is thought to have a toroidal or poloidal shape and to change sign above and below the disk [Sun and Reich, 2010]. It has been described with the following formula by [Sun et al., 2008]:

$$B_\phi(R, z) = sign(z) B_0 \frac{1}{(1 + \frac{|z| - z_0}{z_1})^2} \frac{R}{R_0} \exp(-\frac{R - R_0}{R_0}) \tag{1}$$

where $sign(z)$ indicates the sign change of the halo field on both sides of the disk, $z_0 = 1.5$ kpc and $z_1 = 0.2$ kpc when $|z| < z_0$. When $|z| > z_0$, $z_0 = 4$ kpc. Furthermore, $B_0 = 2$ μG and $R_0 = 4$ kpc. Another possibility for the long lifetime of HVCs is the protection other clouds offer. Most HVCs are embedded in a larger cloud of warm low-density structures. This protects them from the hot surrounding halo and also decreases the relative velocity of the HVC with respect to its surrounding medium. This increases the time for Kelvin-Helmholtz instabilities to form. Evidence of this theory can be found in the MS: HVCs in the MS generally have a tail because there is a limited amount of warm gas in the region. However in areas with large amounts of warm gas, HVCs generally have no tail indicating that they have been affected less by the surrounding hot gas. Most HVCs in the Milky Way will not survive the trip all the way to the disk, unless protected by a warmer component and will integrate into the hot halo [Putman et al., 2012].

4 METHODS

To examine how a magnetic field and the shielding of other clouds could slow down the destruction of a high velocity cloud, I used the PLUTO code to perform a series of two-dimensional simulations.

4.1 PLUTO

PLUTO is a piece of software developed to numerically solve systems of differential equations (conservation laws) present in astrophysical fluid dynamics [Mignone et al., 2007]. Two out of the four available physics modules were used for the simulations in this report: classical hydrodynamics (HD) and magnetohydrodynamics (MHD). The code is written in the C programming language and provides solutions to the following general system of conservation laws in 1, 2 or 3 dimensions:

$$\frac{\partial \mathbf{U}}{\partial t} = -\nabla \cdot \mathbf{T}(\mathbf{U}) + \mathbf{S}(\mathbf{U}) \tag{2}$$

Here $\mathbf{U}$ is a vector and can consist of any evolving physical quantities, $\mathbf{T}(\mathbf{U})$ is a rank-2 tensor. The rows of $\mathbf{T}(\mathbf{U})$ represent the fluxes of each component of $\mathbf{U}$. $\mathbf{S}(\mathbf{U})$ represents any number of source terms (e.g a gravitational field) but no source terms were used in this report. In case of the HD physics module, $\mathbf{U}$ and $\mathbf{T}(\mathbf{U})$ become:

$$\mathbf{U} = \begin{pmatrix} \rho \\ \mathbf{m} \\ E \end{pmatrix}, \mathbf{T}(\mathbf{U}) = \begin{pmatrix} \rho\mathbf{v} \\ \mathbf{m}\mathbf{v} + p\mathbf{I} \\ (E+p)\mathbf{v} \end{pmatrix}^{T}, \tag{3}$$

where $\mathbf{m} = \rho\mathbf{v}$ is the momentum density, $\mathbf{I}$ is a 3x3 unit tensor and the total energy density $E = \frac{p}{\Gamma-1} + \frac{|\mathbf{m}|^2}{2\rho}$. $\mathbf{U}$ contains all physical properties that are evolved, which in case of the HD module are: the density (ρ), velocity ($\mathbf{v}$) and pressure (p). In case of the MHD physics module a magnetic field is added, resulting in the following $\mathbf{U}$ and $\mathbf{T}(\mathbf{U})$ vectors:

$$\mathbf{U} = \begin{pmatrix} \rho \\ \mathbf{m} \\ \mathbf{B} \\ E \end{pmatrix}, \mathbf{T}(\mathbf{U}) = \begin{pmatrix} \rho\mathbf{v} \\ \mathbf{m}\mathbf{v} - \mathbf{B}\mathbf{B} + p_t\mathbf{I} \\ \mathbf{v}\mathbf{B} - \mathbf{B}\mathbf{v} \\ (E+p_t)\mathbf{v} - (\mathbf{v}\cdot\mathbf{B})\mathbf{B} \end{pmatrix}^{T}, \tag{4}$$

with the total pressure $p_t = p + \frac{|\mathbf{B}|^2}{2}$, including both the thermal as well as the magnetic pressure. The energy density in this case becomes
$E = \frac{p}{\Gamma-1} + \frac{1}{2}(\frac{|\mathbf{m}|^2}{\rho} + |\mathbf{B}|^2)$. The numerical integration of these conservation laws is achieved in three steps: a reconstruction phase followed by a Riemann problem at the cell boundaries and an evolution stage.

4.1.1 Reconstruction

PLUTO is grid-based and so evaluates the average of the physical properties of $\mathbf{U}$ in each cell. The flux is evaluated at the interface between each pair of cells. When using only the values of the physical variables in the two adjacent cells this is a first order accurate approximation. To increase the accuracy of the approximation, the values at the interface are instead interpolated based on the values in surrounding cells. The interpolation can be done with either a first order polynomial (linear reconstruction used in this report) or a second order polynomial (parabolic reconstruction). The slope of this polynomial is then limited to avoid very steep gradients between cells with very different values. This increases the stability of the simulations compared to other schemes like Lax-Wendroff.

4.1.2 Riemann solver

The Riemann solver estimates the flux between pairs of cells by solving a Riemann problem. A Riemann problem is posed to find the physical variables at the interface between two cells. These variables can then be used to estimate the flux between the two cells. The exact solution is a combination of waves. The difference between the HLLC and HLLD solver is that they approximate the exact solution by using a different number of waves: 3 in case of the HLLC solver and 5 in case of the HLLD solver.

4.1.3 Evolution

When the fluxes have been determined, the cells can be updated every time-step. There are different approaches to determine an appropriate time-step. In this report the HANCOCK time-stepping method was used. The HANCOCK time-stepping method, HLLC/HLLD Riemann solvers and linear reconstruction methods were chosen because they provide a good balance between accuracy and stability for the simulations.

4.2 SIMULATIONS

The first simulation consisted of a circular cloud of radius 0.5 kpc moving through a rectangular medium with dimensions of 10 by 25 kpc. Both the medium as well as the cloud are considered to be ideal gasses with adiabatic index $\gamma = \frac{5}{3}$. Here the assumption was made that the gas in the cloud as well as the medium is monatomic due to the high temperatures. The medium represents the hot galaxy halo that surrounds the cloud. It has a lower particle density of 0.001 cm^{-3} but a higher temperature of 10^6 K than the cloud such that initially the halo gas and cloud are in pressure equilibrium. These values are consistent with expected physical properties of the halo at the distance where most HVCs are present (2-15 pc) [Putman et al., 2012]. The cloud was given typical properties of high velocity clouds: a temperature of 10^4 K, a velocity of 150 km s^{-1} and a number density of 0.1 cm^{-3} which, around the cloud-halo boundary, gradually decreases to the density of the surrounding medium. To obtain this smooth transition, the following profile was used [Grønnow et al., 2018] :

$$n(r) = n_h + \frac{1}{2}(n_c - n_h)(1 - \tanh(s(\frac{r}{r_c} - 1))), \qquad (5)$$

where $n(r)$ is the number density as a function of the radius of the cloud, n_h is the density of the halo, n_c is the density of the cloud, s is the steepness of the profile, which was set to 10 in this case, and r_c is the radius where the density is halfway between the cloud and halo density. To follow the destruction of the cloud over time, a tracer was added to each cell. Cells inside the cloud are given a value of 1, outside the cloud cells are given a value of 0. The mixing fraction was calculated to quantify the dispersion of the cloud. It is defined as the total mass of gas in mixed cells divided by the total mass of all cloud material in the simulation. It is assumed that a cell is mixed when the tracer of the cell Cis such that: $0.1 < C < 0.9$, this means that at least 10% of the mass of the gas in the cell has a different origin than the rest of the material. In this simulation, where all cells are equal in size, the mixing fraction becomes the following:

$$f_{mix} = \frac{\sum_i \rho_{mix} tr_{mix}}{\sum_i \rho_i tr_{tot}} \qquad (6)$$

Here tr_{mix} are the tracer values for mixed cells and tr_{tot} are all tracer values. This single cloud simulation was then compared to more elaborate simulations containing multiple clouds and/or a magnetic field. All simulations ran for 500 Myr but some adjustments had to be made to run different simulations. In MHD simulations, a magnetic field with a strength of 0.1 μG was implemented perpendicular to the motion of the cloud. Furthermore, in multiple cloud simulations some alterations were made to the grid size. In order to give all clouds enough space to move, the grid was increased in size to 35 by 10 kpc. The distance between cloud centers was set to be 4 kpc which equals 4 times the diameter of the clouds. The same tracer was added separately to each individual cloud in multiple cloud simulations so the destruction of the clouds in different simulations could be compared.

5 RESULTS

The output of the simulations was visualized using python. Unfortunately the simulation running the single cloud could only be used up until 250 Myr because the cloud material already started to escape through the far side of the simulated region. Therefore only the first 10 of 20 output files were used for all simulations, to ensure reasonable comparisons. This changed the timescale from 500 Myr to 250 Myr, which turned out to be enough time to destroy the clouds to different degrees.

	Cloud A	Cloud B	Cloud C
HD SC	0.27	-	-
HD MC	0.25	0.18	0.17
MHD SC	0.10	-	-
MHD MC	0.16	0.16	0.09

Table 1: All mixing fractions at t = 250 Myr. (SC = single cloud, MC = multiple cloud)
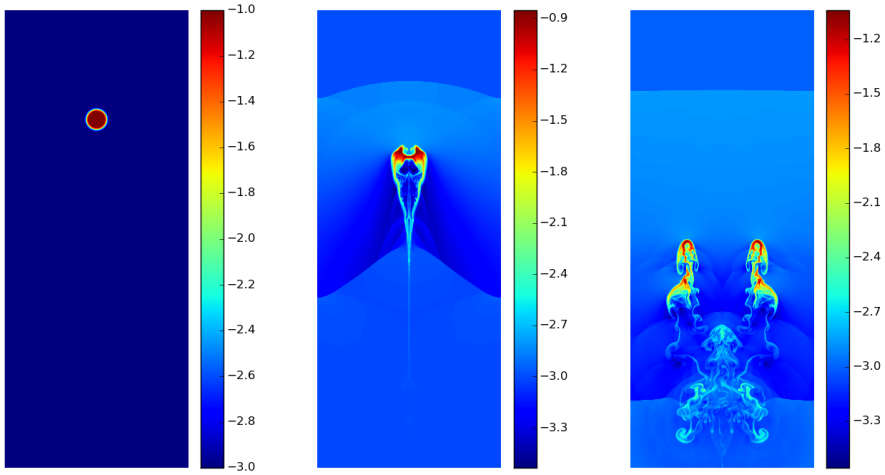

Figure 4: Single cloud evolution: the logarithm of the density in units of atomic mass cm^{-2} displays the evolution of the cloud at t = 0 Myr (left panel), t = 125 Myr (middle panel) and t = 250 Myr (right panel).

As seen in figure 4, the single cloud forms a tail around 125 Myr into its lifetime. At t = 250 Myr, the cloud is mostly destroyed and its mixing fraction has reached a value of 0.27. In addition, the cloud has split into two separate parts. This has been seen in other simulations and caused by Raleigh-Taylor instabilities [Grønnow et al., 2018]. The acceleration of the cloud acts in a similar way to gravitational acceleration and combined with the density difference this creates an instability eroding away the middle of the cloud. This effect results in the cloud splitting up.
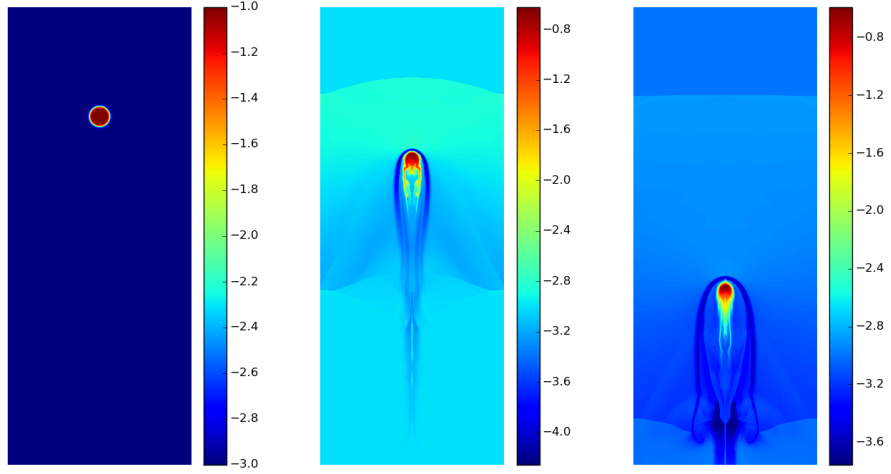
Figure 5: MHD simulation showing the logarithm of the density of a single cloud at t = 0 (left panel), t = 125 (middle panel) and t = 250 Myr (right panel), in units of atomic mass cm^{-2}.
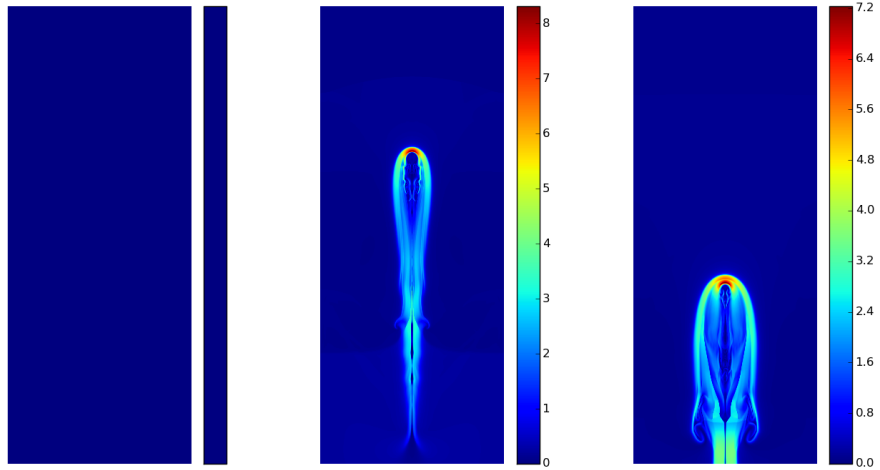

Figure 6: The magnetic field evolution corresponding to figure 5, showing the draping of the magnetic field in case of a single cloud. The strength of the magnetic field is given in μG

In figure 5 the same simulation was done with the addition of a magnetic field perpendicular to the motion of the cloud. As can be seen in the figure, this has some very noticeable effects on the

16

evolution of the cloud. It no longer splits in two but remains whole during the whole simulation. The cloud does form a tail but does not seem to completely fall apart in 250 Myr. This can be inferred from the low mixing fraction as well: after 250 Myr it's mixing fraction has reached a value of 0.10. In addition, the magnetic field creates a low density area surrounding the cloud. This area is formed because of the deformation of the magnetic field. As can be seen in figure 6, the cloud acts as an obstacle to the magnetic field. The magnetic field drapes around the cloud and accumulates around it. It reaches the highest values right in front of it (around 7 μG) and weakens slightly to the sides and behind the cloud (around 3 μG). Because in these areas the magnetic field is so strong, the total pressure (consisting of a thermal and magnetic component) increases as well. This causes the gas to be pushed out of the region until the total pressure returns to an equilibrium with the surrounding region. This creates very low density areas where the magnetic field is strongest.
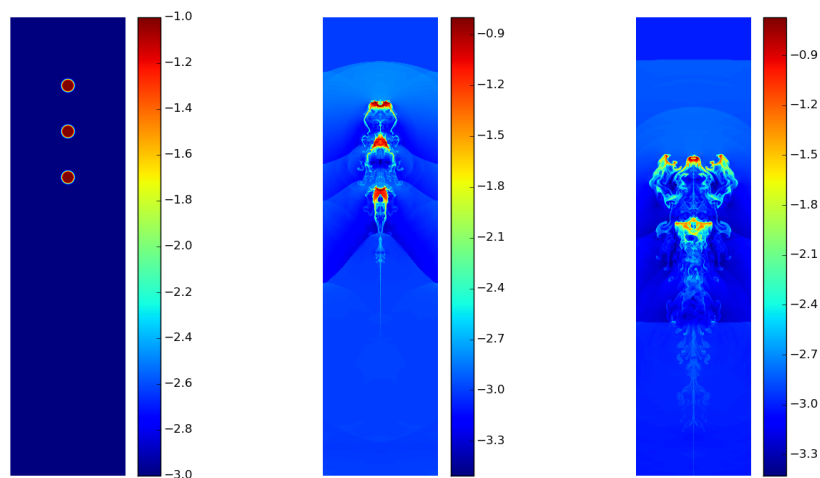

Figure 7: Multiple cloud evolution: In this figure the logarithm of the density in units of atomic mass cm^{-2} displays the destruction of three aligned clouds at t = 0 Myr (left panel), t = 125 Myr (middle panel) and t = 250 Myr (right panel).

When looking at figure 7 it can clearly be seen that, in a simulation with three clouds, the first cloud (cloud A) behaves very similar to the single cloud from the base simulation: it splits in two and is close to being destroyed after 250 Myr. However, the second and third cloud (cloud B and C) are more interesting. Cloud B is initially protected by cloud A in front of it. Cloud A is then split in two and decelerated by the interaction with the halo. In the reference frame of cloud A, Cloud B which has a slightly higher velocity due to it having a limited interaction with halo material, then moves towards cloud A. After 250 Myr, cloud B has closed the gap to cloud A and has moved in between the two separate clouds created by the splitting of cloud A. which is why it seems as if only 2 clouds are present in the third time frame of figure 7. To study the destruction of the clouds, the mixing fractions of the 3 clouds are compared separately to the mixing fraction of the single cloud from figure 4.
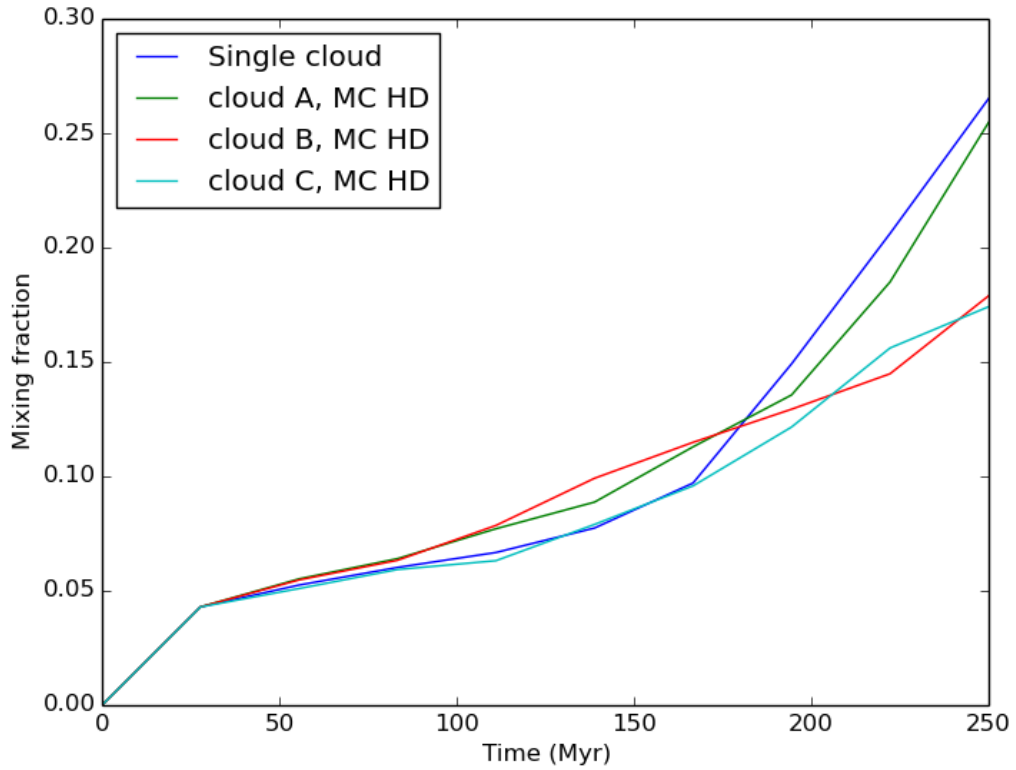
Figure 8: A comparison of the mixing fractions of the cloud from the HD single cloud simulation and individual clouds from the HD multiple cloud simulation.

As can be seen in figure 8, the mixing fraction of cloud A evolves very similar to the single cloud from figure 4 (0.25 after 250 Myr). Cloud B and C however, have a significantly lower mixing fraction because they were shielded from the hot halo by cloud A. Cloud C does not seem to benefit from the additional protection of cloud B, as the mixing fraction of cloud B and C are very similar: Cloud B has a mixing fraction of 0.18 after 250 Myr compared to 0.17 for cloud C.
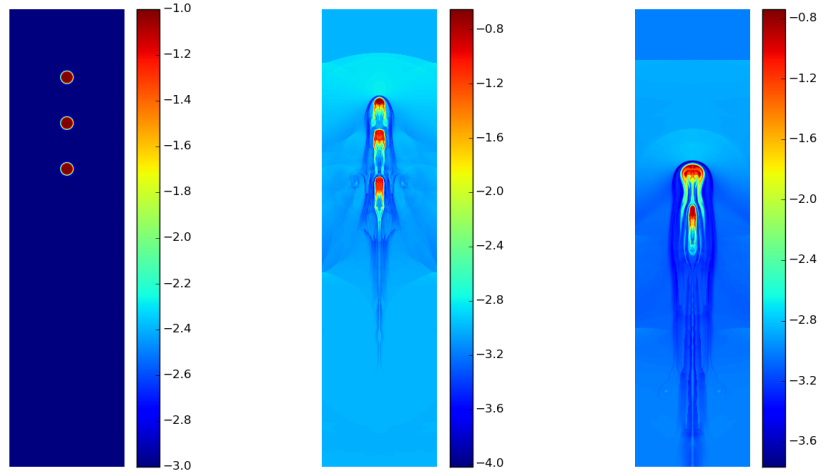
Figure 9: Multiple cloud with magnetic field evolution: In this figure the logarithm of the density in units of atomic mass cm^{-2} displays the destruction of three aligned clouds at t = 0 Myr (left panel), t = 125 Myr (middle panel) and t = 250 Myr (right panel).
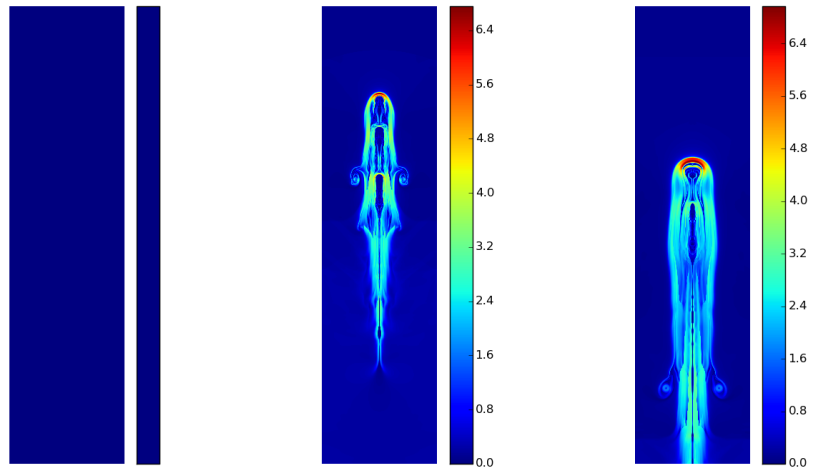

Figure 10: The magnetic field evolution corresponding to figure 5, showing the draping of the magnetic field in case of multiple clouds. The magnetic field strength is given in μG.

In the final simulation, where the effects of shielding by other clouds and a magnetic field are combined, the clouds seem to be preserved best. As seen in the multiple cloud simulation, cloud A evolves similarly to the single cloud with magnetic field. Cloud B, being protected by cloud A, moves faster and moves towards cloud A much like in the multiple cloud simulation without magnetic field. Because in this case cloud A is stabilized by the magnetic field, cloud B cannot move any further and merges with cloud A. Cloud C is then protected by the first two clouds and will move towards these clouds. To compare if the addition of a magnetic field prolongs the lifetime of cloud B and C compared to cloud B and C of the simulation without magnetic field, their mixing fractions are studied. The mixing fraction of cloud B and C in case of the multiple cloud simulation with and without magnetic field is also compared to the single cloud simulation with magnetic field to estimate whether the addition of other clouds has any extra effect. For simplicity, the first cloud of both the multiple cloud simulations is not displayed in the figure because they behave very similar to the single cloud variations.
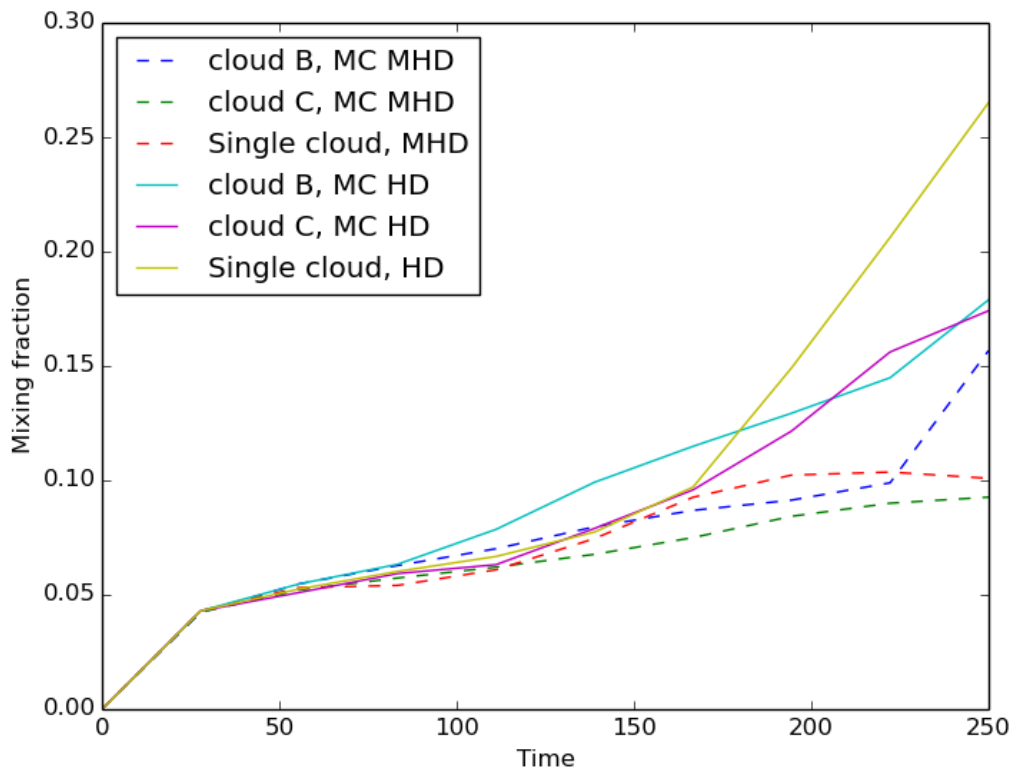
Figure 11: The mixing fraction compared for all clouds over their lifetime. (MCBF = multiple cloud with magnetic field, BF is single cloud with magnetic field, MC = multiple cloud)

From figure 11 it is clear that both the magnetic field as well as the shielding of other clouds affect the lifetime of HVCs. However, their combined effect results in a similar mixing fraction to the single cloud with a magnetic field. After 250 Myr, cloud C has reached a mixing fraction of 0.09 compared to a mixing fraction of 0.10 for the magnetic field simulation. Cloud B reaches a mixing fraction of 0.16, this is closer to the mixing fractions of cloud B and C of the multiple cloud simulation. This result can be explained by studying figure 10 which shows the magnetic field evolution in the multiple cloud case. In the third time frame, cloud C has moved close enough to cloud B that it disrupts its tail. This results in a sudden increase of the mixing fraction of cloud B, as can be seen in figure 11: The mixing fraction of cloud B in the multiple cloud magnetic field case (MCBF in the figure) has a steep increase around 225 Myr into its lifetime. Around this time, cloud C has gotten close enough to start disrupting the tail of cloud B.

6 DISCUSSION

The results presented in this report show that a magnetic field (by preventing the formation of Kelvin-Helmholtz instabilities) as well as the shielding effect from other clouds can prolong the lifetime of HVCs. Of these two, I found the effect of the magnetic field to be significantly larger. However, the combined effect of these two did not result in a better preserved cloud than the case of just a magnetic field. It is not clear how general this trend is because only one set of simulations was done. More simulations have to be run to get an accurate representation of the evolution of HVCs in the galactic halo. For example, all simulations have been done in two dimensions. This results in the clouds having a much smaller surface area perpendicular to the motion of the cloud than a spherical cloud. This reduces chances for instabilities to develop and so increases the lifetime of the cloud compared to more accurate 3D simulations [Grønnow et al., 2018]. The magnetic field in the galactic halo can vary between negligible and 2 μG [Sun and Reich, 2010]. In the simulations the magnetic field was set to be 0.1 μG, this spans a very small region of the values the magnetic field could actually have. The simulations also all assumed the same velocity: 150 km/s. While this is possible for a HVC, the velocity of HVCs ranges up to 400 km s^{-1} compared to the surrounding halo [Olano, 2008]. Velocities above 150 km s^{-1} were not tested because the simulations became unstable for supersonic speeds. Variations in magnetic field strength, cloud velocities and three dimensional simulations should give a better perspective on HVC lifetimes. However, the simulations in this report do have implications for gas accretion: both the shielding effect as well as the suppression of instabilities by the magnetic field significantly prolongs the life time of HVCs. For clouds in the outer halo, where the magnetic field is very weak, the shielding of other clouds is the dominant effect. In this area the multiple cloud simulation is the most representative, showing that the shielding affect can increase the amount of cold gas reaching the inner parts of the halo. For clouds closer to the galactic disk that have survived the journey from the outer parts of the halo or originate from fountain accretion, I found the magnetic field to be the dominant effect. From the MHD simulations it is clear that the strong magnetic field in the inner halo can greatly increase the lifetime of HVCs, whether they are protected by other clouds or not. Overall, significantly more gas is able to reach the star forming disk because of these effects.

7 CONCLUSION

It is clear that both the shielding of other clouds as well as the magnetic field of the halo prolonges the lifetime of HVCs. The largest effect is caused by the magnetic field. The mixing fraction of the MHD single cloud simulation was found to be nearly half of the mixing fraction of cloud B and C in the HD multiple cloud simulation after 250 Myr. The MHD multiple cloud simulation did not prolong the lifetime of the clouds any further based on their mixing fraction: the mixing fraction of the MHD single cloud and MHD multiple cloud simulations was almost the same for cloud B of the multiple cloud simulation Cloud B actually had a higher mixing fraction than the MHD single cloud, most likely due to cloud C disrupting the tail of cloud B in this case. In gas halo regions where the magnetic field is weak, such as the outer parts far removed from the star-forming disk, the shielding of other clouds is the dominant effect. In areas closer to the star-forming disk, the magnetic field is stronger and becomes the more dominant effect. Overall both provide enough protection for the HVCs such that a significantly larger portion of cold gas reaches the star-forming disk. To examine the importance of this in detail, more simulations need to be done and simulations would need to be performed in 3D. Variations in the velocity, density and size of the HVCs need to be examined as well as different magnetic field strengths plausible in the halo.

References

J. S. Almeida. Gas Accretion and Star Formation Rates. 2016. doi: 10.1007/978-3-319-52512-9$_4$.

M. Cousin, P. Guillard, and M. D. Lehnert. G.A.S. I. A prescription for turbulence-regulated star formation and its impact on galaxy properties. *Astronomy and Astrophysics*, 2019. doi: 10.1051/0004-6361/201834673.

K. Finlator and R. Davé. The origin of the galaxy mass–metallicity relation and implications for galactic outflows. *Monthly Notices of the Royal Astronomy Society*, 385:2181–2204, 2008. doi: https://doi.org/10.1111/j.1365-2966.2008.12991.x.

A. Grønnow, T. Tepper-García1, and J. Bland-Hawthorn. Magnetic Fields in the Galactic Halo Restrict Fountain-driven Recycling and Accretion. *The astrophysical journal*, 865(64):1–17, 2018. doi: https://doi.org/10.3847/1538-4357/aada0e.

G. G. Kacprzak. Gas Accretion in Star-Forming Galaxies. 2016. doi: 10.1007/978-3-319-52512-9$_7$.

D. Keres, N. Katz, D. H. Weinberg, and R. Dave. How Do Galaxies Get Their Gas? *Monthly Notices of the Royal Astronomy Society*, 363:2–28, 2005. doi: 10.1111/j.1365-2966.2005.09451.x.

N. Lehner, J. C. Howk, C. Thom, A. J. Fox, J. Tumlinson, T. M. Tripp, and J. D. Meiring. High-velocity clouds as streams of ionized and neutral gas in the halo of the Milky Way. *Monthly Notices of the Royal Astronomical Society*, 424:2896–2913, 2012. doi: 10.1111/j.1365-2966.2012.21428.x.

A. Marasco, F. Fraternali, and J. J. Binney. Supernova-driven gas accretion in the Milky Way. *Monthly Notices of the Royal Astronomical Society*, pages 1107–1120, 2012. doi: 10.1111/j.1365-2966.2011.19771.x.

A. Mignone, G. Bodo, S. Massaglia, T. Matsakos, O. Tesileanu, C. Zanni, and A. Ferrari. PLUTO: A Numerical Code for Computational Astrophysics. *The Astrophysical Journal Supplement Series*, 170:228–242, 2007. doi: 10.1086/513316.

M. J. Miller and J. N. Bregman. The Structure of the Milky Way's Hot Gas Halo. 2013. doi: 10.1088/0004-637X/770/2/118.

C. A. Olano. Distribution of the high-velocity clouds in the Galactic halo. *Astronomy and Astrophysics*, 485:457–473, 2008. doi: 10.1051/0004-6361:20077556.

M. E. Putman, J. E. G. Peek, and M. R. Joung. Gaseous Galaxy Halos. *Annual Review of Astronomy and Astrophysics*, 50:491–529, 2012. doi: 10.1146/annurev-astro-081811-125612.

R. Sancisi, F. Fraternali, T. Oosterloo, and T. van der Hulst. Cold gas accretion in galaxies. *Astronomy and Astrophysics Reviews*, 15:189–223, 2008. doi: 10.1007/s00159-008-0010-0.

X. H. Sun and W. Reich. The Galactic halo magnetic field revisited. 2010. doi: 10.1088/1674-4527/10/12/009.

X. H. Sun, W. Reich, A. Waelkens, and T. A. Enßlin. Radio observational constraints on Galactic 3D-emission models. *Astronomy and Astrophysics*, pages 573–592, 2008. doi: 10.1051/0004-6361:20078671.

T. Tepper-García, J. Bland-Hawthorn, M. S Pawlowski, and T. K Fritz. The Magellanic System: the puzzle of the leading gas stream. *Monthly notices of the Royal Astronomy Society*, 488:918–938, 2019. doi: https://doi.org/10.1093/mnras/stz1659.

C. Thom, J. E. G. Peek, M. E. Putman, Carl Heiles, K. M. G. Peek, , and R. Wilhelm. An Accurate Distance to High-Velocity Cloud Complex C. *The Astrophysical Journal*, 684:364–372, 2008. doi: https://doi.org/10.1086/589960.

J. Tumlinson, M. S. Peeples, and J. K. Werk. The Circumgalactic Medium. *Annual Review of Astronomy and Astrophysics*, 55:389–432, 2017. doi: https://doi.org/10.1146/annurev-astro-091916-055240.

B. P. Wakker and H. van Woerden. HIGH-VELOCITY CLOUDS. *Annual Review of Astronomy and Astrophysics*, 35:217–266, 1997.

T. Westmeier. A new all-sky map of Galactic high-velocity clouds from the 21-cm HI4PI survey. *Monthly Notices of the Royal Astronomical Society*, 474:289–299, 2018. doi: https://doi.org/10.1093/mnras/stx2757.